An Application of Kalman Techniques to Aircraft and Missile Radar Tracking

G. T. ALDRICH*
AII Systems, Moorestown, N.J.
AND
W. B. KRABILL†
NASA, Wallops Island, Va.

A real-time and postflight data reduction and error analysis program is developed with the ability to estimate either aircraft flight paths or missile trajectories with the same state vector and matrix dimension filter equations simply by input selection of the appropriate state transition matrix. A feature of the filter formulation is an analytical technique for computing the effects of measurement error parameters not explicitly included in the filter state vector on both the state vector estimate itself and the state covariance matrix. Examples of the processing of real tracking data for aircraft flight paths, missile trajectories, and some other more unusual applications are presented which illustrate both the data reduction and error analysis modes of program operation.

Introduction

THE NASA Wallops Station is responsible for providing aircraft, missile and satellite tracking facilities for the purpose of providing a standard against which the performance of airborne navigation, control and sensor equipment can be evaluated. The quality of the tracking range standard is dependent on both the data processing procedure used and the errors introduced by the tracking range sensors. The objective of the effort reported herein was to develop a single tracking data reduction program suitable for both aircraft flight paths and missile trajectories, both real-time traffic management and postmission analysis applications, and a tracking sensor error analysis for both systematic and random measurement errors. The Kalman filter program (KAPPA) is applied herein to the case of a single tracking radar (range, azimuth and elevation measurements), but is readily adaptable to other single or combination tracking sensor (radars, beacons, theodolites, lasers, etc.) configurations.

The development of the filter includes several features from which it derives its versatility. The first of these features is the ability to estimate either aircraft flight paths or missile powered and coasting trajectories with the same state vector and matrix dimension filter equations simply by input selection of the appropriate state transition matrix. The filter formulation also includes an adaptive bandwidth feature which permits the detection of high-frequency dynamic transients (aircraft touchdown, missile staging, etc.) and provides closed-loop control of the filter bandwidth through residual feedback to the state noise matrix.

Another feature of the filter formulation is the development of an analytical technique for computing the effects of measurement error parameters not explicitly included in the filter state vector (bias, timing, scale factor, location, etc.) on both the state vector estimate itself and the state covariance matrix. This technique permits calculation of these effects without increasing the dimension of the filter state vector (filter per cycle running time is approximately proportional to the cube of the state vector dimension) for real-time applications as well as operation of the filter in an error analysis mode for postmission data analysis application. This error analysis technique requires the computation of only one matrix (a matrix of partials of the measurements with respect to the measurement errors) which is not already computed in any standard Kalman filter formulation. The effect of the measurement errors on both the state vector estimate itself and on the state covariance matrix can then be computed from linear operations involving the new matrix and other matrices already computed.

The Kalman filter program (KAPPA) described in this paper has been implemented on a HW-625 computer at NASA Wallops Station. There are two versions of the program, both written in FORTRAN IV. One is a streamlined version that cycles in approximately 25 msec. The second is a postmission data processing tool. The postmission version operates entirely in double precision, and has a variety of optional outputs to aid the data analyst and scientific investigator.

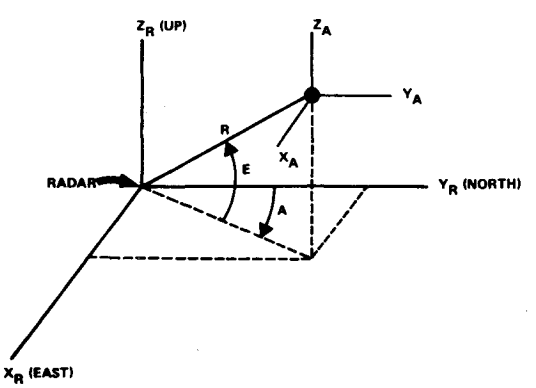

Fig. 1 KAPPA coordinate systems.

Presented as Paper 72-838 at the AIAA Guidance and Control Conference, Stanford, Calif., August 14–16, 1972; submitted September 18, 1972; revision received January 30, 1973. The work reported in this paper was accomplished while G. T. Aldrich was Manager, Navigation and Control, Wolf Research and Development Corporation, Riverdale, Md.

Index categories: Air Navigation, Communication, and Traffic Control Systems; LV/M Trajectories; Navigation, Control, and Guidance Theory.

* Director, Software and Analysis. Member AIAA.
† Manager, Navigation and Traffic Control Programs.

Mathematical Formulation

State Dynamic Models

In order to achieve the objective of developing a single Kalman filter program with the capability to estimate both aircraft flight paths and missile powered and coasting trajectories with the same state vector and matrix dimension filter equations, it was necessary to formulate separate state dynamic models which were similar, but which provided a satisfactory mathematical description of both kinds of flight. Figure 1 illustrates the coordinate systems used.

R, A, and E are the radar polar coordinates with origin at the radar. R is the range from the radar to the aircraft or missile, A is the azimuth angle (measured positive from north clockwise) and E is the elevation angle (measured positive upward from horizontal). Radar measurements are made in this system.

X_R, Y_R, and Z_R are the radar Cartesian coordinates with origin at the radar. X_R and Y_R lie in the horizontal plane with Y_R directed north and X_R directed east. Z_R completes the right-handed set and is directed upward along the local vertical. KAPPA input and output are in this system.

X_A, Y_A and Z_A are the aircraft or missile Cartesian coordinates with origin at the center of gravity. This coordinate system translates with the aircraft or missile, but does not rotate. X_A, Y_A, and Z_A remain parallel to X_R, Y_R, and Z_R at all times. The aircraft and missile equations of motion are written in this system.

Consider the aircraft or missile velocity vector shown in the aircraft or missile Cartesian coordinate system in Fig. 2. Resolving the velocity vector into the Cartesian coordinate system

$$\dot{X}_A = V\cos\theta\sin\psi, \quad \dot{Y}_A = V\cos\theta\cos\psi, \quad \dot{Z}_A = V\sin\theta \tag{1}$$

and taking the derivative with respect to time of Eqs. (1)

$$\begin{aligned} \ddot{X}_A &= \dot{V}\cos\theta\sin\psi + \dot{\psi}V\cos\theta\cos\psi - \dot{\theta}V\sin\theta\sin\psi \\ \ddot{Y}_A &= \dot{V}\cos\theta\cos\psi - \dot{\psi}V\cos\theta\sin\psi - \dot{\theta}V\sin\theta\cos\psi \\ \ddot{Z}_A &= \dot{V}\sin\theta + \dot{\theta}V\cos\theta \end{aligned} \tag{2}$$

At this point it was necessary to begin to differentiate between aircraft and missile dynamic behavior as will be done below.

Aircraft

Because of the high measurement data rate of the Wallops radars (10 points per second), reasonable aircraft dynamic behavior will allow the assumptions of constant acceleration ($\ddot{V} = 0$), constant glideslope angle ($\dot{\theta} = 0$) and constant bank angle ($\dot{\phi} = 0$) between data points. Assuming also that the aircraft turn is coordinated by the pilot

$$\dot{\psi} = (g/V)\tan\phi \tag{3}$$

Substituting (1) and (3) into (2)

$$\ddot{X} = \dot{V}\dot{X}/V + g\tan\phi\dot{Y}/V, \quad \ddot{Y} = \dot{V}\dot{Y}/V - g\tan\phi\dot{X}/V, \quad \ddot{Z} = \dot{V}\dot{Z}/V \tag{4}$$

Note that the subscript A has been dropped, since Eqs. (4) are also true in the radar Cartesian coordinate system. Equations (4) represent a vector state equation of the desired form

$$\dot{\bar{X}} = \bar{F}(\bar{X}) \tag{5}$$

The continuous state representation of Eq. (5) can be discretized for arbitrary Δt to arrive at the matrix equation below:

$$\begin{bmatrix} X \\ Y \\ Z \\ \dot{X} \\ \dot{Y} \\ \dot{Z} \\ \dot{V} \\ \tan\phi \end{bmatrix}_n = \begin{bmatrix} X_1 \\ X_2 \\ X_3 \\ X_4 \\ X_5 \\ X_6 \\ X_7 \\ X_8 \end{bmatrix}_n = \begin{bmatrix} 1 & 0 & 0 & \Delta t & 0 & 0 & \frac{X_4\Delta t^2}{2V} & \frac{gX_5\Delta t^2}{2V} \\ 0 & 1 & 0 & 0 & \Delta t & 0 & \frac{X_5\Delta t^2}{2V} & -\frac{gX_4\Delta t^2}{2V} \\ 0 & 0 & 1 & 0 & 0 & \Delta t & \frac{X_6\Delta t^2}{2V} & 0 \\ 0 & 0 & 0 & 1 & 0 & 0 & \frac{X_4\Delta t}{V} & \frac{gX_5\Delta t}{V} \\ 0 & 0 & 0 & 0 & 1 & 0 & \frac{X_5\Delta t}{V} & -\frac{gX_4\Delta t}{V} \\ 0 & 0 & 0 & 0 & 0 & 1 & \frac{X_6\Delta t}{V} & 0 \\ 0 & 0 & 0 & 0 & 0 & 0 & 1 & 0 \\ 0 & 0 & 0 & 0 & 0 & 0 & 0 & 1 \end{bmatrix}_{n/n-1} \begin{bmatrix} X_1 \\ X_2 \\ X_3 \\ X_4 \\ X_5 \\ X_6 \\ X_7 \\ X_8 \end{bmatrix}_{n-1} \tag{6}$$

$$V = (X_4^2 + X_5^2 + X_6^2)_{n-1}^{1/2}$$

The inclusion of $\tan\phi$ as a state element significantly improves the accuracy of the state dynamic model when the filter is applied to tracking data obtained from maneuvering aircraft. Further, for certain applications at Wallops Station, aircraft bank angle is a desired solution state.

Missiles

Starting again with Eqs. (2), missile trajectories typically feature rapid acceleration changes at burnout, staging, etc. Most of this rapid acceleration change occurs in the direction of the velocity vector due to thrust and drag changes, rather than due to a turning of the velocity vector. Again, noting the high measurement data rate, the expected missile dynamic behavior will therefore allow the assumptions of constant rate of change of acceleration ($\dddot{V} = 0$) and constant velocity vector direction ($\dot{\theta} = \dot{\psi} = 0$) between data points. Differentiating (2) again and substituting (1)

$$\dddot{X} = \dot{V}\dot{X}/V, \quad \dddot{Y} = \dot{V}\dot{Y}/V, \quad \dddot{Z} = \dot{V}\dot{Z}/V \tag{7}$$

Proceeding as with Eqs. (5) and (6), and including a central force-field gravity model, it can be shown that

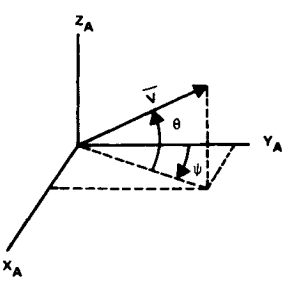

Fig. 2 Velocity in aircraft or missile Cartesian coordinates.

$$\begin{bmatrix} X \\ Y \\ Z \\ \dot{X} \\ \dot{Y} \\ \dot{Z} \\ \dot{V} \\ \dot{V} \end{bmatrix}_n = \begin{bmatrix} X_1 \\ X_2 \\ X_3 \\ X_4 \\ X_5 \\ X_6 \\ X_7 \\ X_8 \end{bmatrix}_n = \begin{bmatrix} 1-\frac{GM}{R^3}\frac{\Delta t^2}{2} & 0 & 0 & \Delta t & 0 & 0 & \frac{X_4\Delta t^2}{2V} & \frac{X_4\Delta t^3}{6V} \\ 0 & 1-\frac{GM}{R^3}\frac{\Delta t^2}{2} & 0 & 0 & \Delta t & 0 & \frac{X_5\Delta t^2}{2V} & \frac{X_5\Delta t^3}{6V} \\ 0 & 0 & 1-\frac{GM}{R^3}\frac{\Delta t^2}{2} & 0 & 0 & \Delta t & \frac{X_6\Delta t^2}{2V} & \frac{X_6\Delta t^3}{6V} \\ -\frac{GM}{R^3}\Delta t & 0 & 0 & 1 & 0 & 0 & \frac{X_4\Delta t}{V} & \frac{X_4\Delta t^2}{2V} \\ 0 & -\frac{GM}{R^3}\Delta t & 0 & 0 & 1 & 0 & \frac{X_5\Delta t}{V} & \frac{X_5\Delta t^2}{2V} \\ 0 & 0 & -\frac{GM}{R^3}\Delta t & 0 & 0 & 1 & \frac{X_6\Delta t}{V} & \frac{X_6\Delta t^2}{2V} \\ 0 & 0 & 0 & 0 & 0 & 0 & 1 & \Delta t \\ 0 & 0 & 0 & 0 & 0 & 0 & 0 & 1 \end{bmatrix}_{n/n-1} \begin{bmatrix} X_1 \\ X_2 \\ X_3 \\ X_4 \\ X_5 \\ X_6 \\ X_7 \\ X_8 \end{bmatrix}_{n-1} - \begin{bmatrix} 0 \\ 0 \\ R_E\frac{GM}{R^3}\frac{\Delta t^2}{2} \\ 0 \\ 0 \\ R_E\frac{GM}{R^3}\Delta t \\ 0 \\ 0 \end{bmatrix}_{n-1} \tag{8}$$

$$R = [X_1^2 + X_2^2 + (X_3 + R_E)^2]_{n-1}^{1/2}$$

Filter Formulation

The KAPPA program was implemented using the standard Kalman filter equations[1] shown below for the aircraft case in vector and matrix form

$$\begin{aligned} X_{n/n-1} &= \Phi_{n/n-1} X_{n-1/n-1} \\ S_{n/n-1} &= \Phi_{n/n-1} S_{n-1/n-1} \Phi_{n/n-1}{}^T + Q_n \\ H_n &= S_{n/n-1} M_n{}^T (R_n + M_n S_{n/n-1} M_n{}^T)^{-1} \\ X_{n/n} &= X_{n/n-1} + H_n (Y_n - M_n X_{n/n-1}) \\ S_{n/n} &= (I - H_n M_n) S_{n/n-1} \end{aligned} \tag{9}$$

where the transition matrix, $\Phi_{n/n-1}$, is given by Eq. (6).

The only changes required in order to estimate missile trajectories instead of aircraft flight paths are an input selection option of the transition matrix, $\Phi_{n/n-1}$, from Eq. (8) instead of Eq. (6), and augmentation of the state prediction equation as

$$X_{n/n-1} = \Phi_{n/n-1} X_{n-1/n-1} - \begin{bmatrix} 0 \\ 0 \\ R_E\frac{GM}{R^3}\frac{\Delta t^2}{2} \\ 0 \\ 0 \\ R_E\frac{GM}{R^3}\Delta t \\ 0 \\ 0 \end{bmatrix} \tag{10}$$

Note that for aircraft flight paths the eighth state variable X_8 is the tangent of the aircraft bank angle. For missile trajectories the eighth state variable X_8 is the rate of change of missile acceleration.

Adaptive Bandwidth

Kalman filters suffer from the classic filtering theory problem that they cannot be simultaneously optimized for both steady-state and transient operation. The nature of the mathematical formulation of a Kalman filter causes the gain matrix H_n to grow exponentially smaller with time and, thus, the filter weighs the incoming data lightly relative to the dynamic model after a long period of steady-state operation. Effectively, this means the bandwidth of the filter has grown small. If the object being tracked suddenly maneuvers (transient condition), the filter responds poorly (slowly, if at all) to the transient because of the narrow steady-state bandwidth.

An often used method[1] of avoiding the narrow bandwidth problem is to input a large "state noise" (Q matrix). This action produces the undesirable effect of poor noise suppression during steady-state conditions, however, by keeping the bandwidth too wide. If, however, one can detect transient situations, the Q matrix can be increased in their presence. Similarly, if one can detect steady-state conditions, the Q matrix can be decreased in their presence. Thus, the filter bandwidth can be "adapted" to the dynamic situation. Repeating the state vector update equation

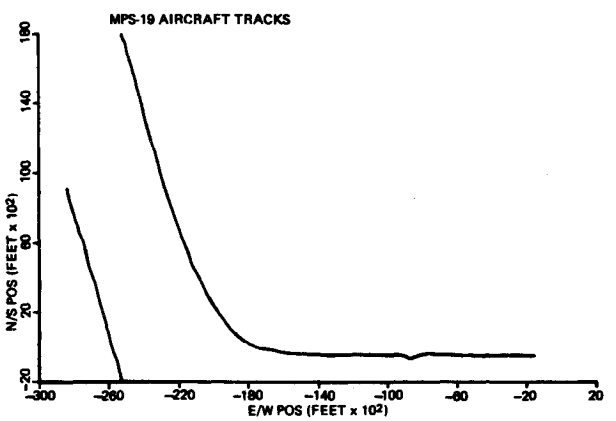

Fig. 3 Aircraft position.

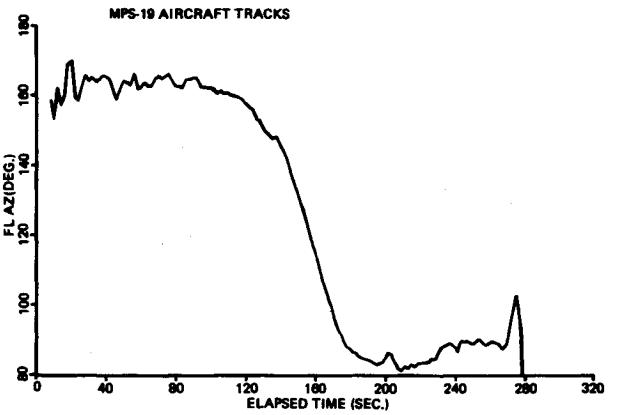

Fig. 4 Aircraft heading.

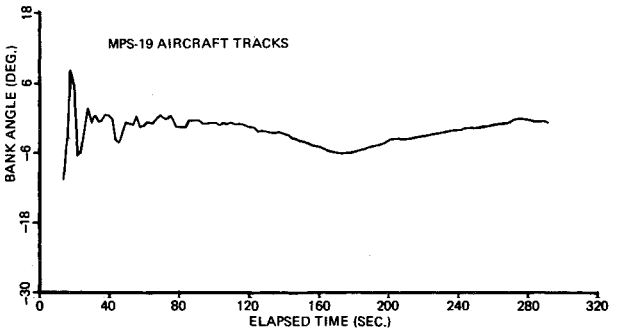

Fig. 5 Aircraft bank angle.

$$X_{n/n} = X_{n/n-1} + H_n(Y_n - M_n X_{n/n-1}) \tag{11}$$

The term in parentheses is the residual between the actual and the predicted measurements. A sudden increase in this term would indicate a transient dynamic situation. This term is sensitive to measurement noise, however, since noise is contained in the measurements Y_n.

If Eq. (11) is rewritten

$$X_{n/n} - X_{n/n-1} = H_n(Y_n - M_n X_{n/n-1}) \tag{12}$$

the term on the left-hand side of Eq. (12) represents the residual between the smoothed estimate and the predicted estimate. A sudden or prolonged increase in this term is more likely due to transient dynamics. Similarly, this term is small during steady-state dynamics. Using this term to detect a transient vs a steady-state dynamic situation introduces a smoothing lag, but overcomes undue sensitivity to measurement noise.

A simple method of using this term to "adapt" the filter bandwidth to the dynamic situation as shown below was mechanized in KAPPA

$$Q_n = K_1 H_n(Y_n - M_n X_{n/n-1})(Y_n - M_n X_{n/n-1})^T H_n{}^T + K_2 Q_{n-1}$$
$$Q_{i \neq j} = 0 \tag{13}$$

Thus, the Q matrix input at each data point is a function of both the previous Q matrix and the smoothed residual. Q_n gets large in transient situations and small in steady-state ones. K_1 and K_2 are input weighting gains.

Error Analysis Formulation

The filter formulation, Eqs. (9), assumes that the observation model has the form

$$Y_n = M_n X_n + V_n \tag{14}$$

such that the vector of measurements Y_n consists of a term which is determined by the state X_n plus a vector of zero-mean random noise V_n. If nonobservable systematic errors (range and angle biases, timing bias, location bias, etc.) are known to exist, they are normally included in the state vector, propagated with an identity transition matrix, and their operation on themselves set to zero in the Kalman gain matrix.[2] Thus the Kalman gain and covariance matrices are optimal and correct, respectively, for the observable state variables. This method of accounting for nonobservable systematic errors increases the state vector dimension, increases the number of matrix multiplications, and, hence, increases program running time (even with conventional partitioning).

A method has been proposed[3] which will allow the separate calculation of the contribution of nonobservable systematic errors in a single set of measurements at a single time point on the state estimate. This method does not allow the calculation of the total effect of nonobservable systematic errors in all the measurements up to the present time on the present state estimate, however. This method was based on earlier work[4] done for batch least-squares applications. The following derivation extends Ref. 3 using the techniques in Ref. 4 as applied to sequential estimation.

Consider a different formulation of the measurement equation:

$$Y_n = M_n X_n + K_n \gamma_n + V_n \tag{15}$$

where X_n now contains only observable state variables, and γ_n is a vector of nonobservable systematic errors related by K_n, a matrix of partial derivatives of the measurements with respect to the nonobservable systematic errors, to the measurements.

The actual (not estimated) state is given by

$$X_n = \Phi_{n/n-1} X_{n-1} + W_n \tag{16}$$

where W_n is a vector of state noise.

The filter predicts the state using

$$X_{n/n-1} = \Phi_{n/n-1} X_{n-1/n-1} \tag{17}$$

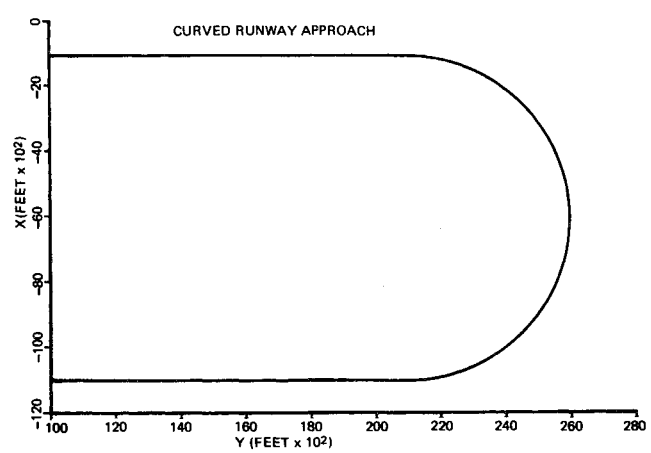

Fig. 6 Aircraft position, simulated data.

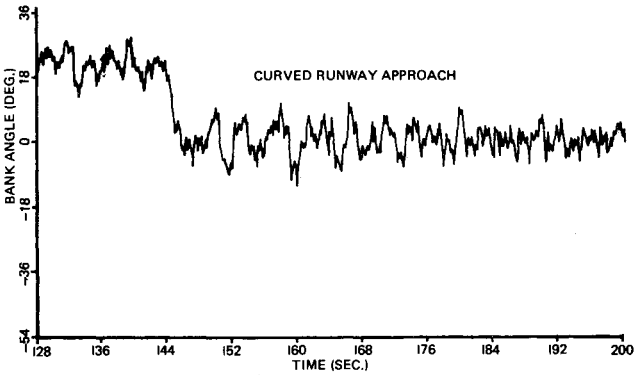

Fig. 7 Aircraft bank angle, simulated data, high adaptability.

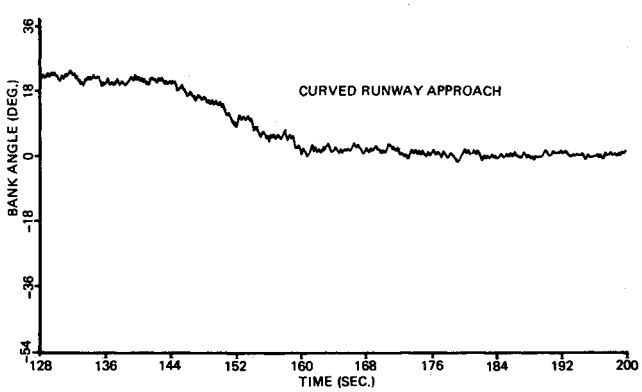

Fig. 8 Aircraft bank angle, simulated data, low adaptability.

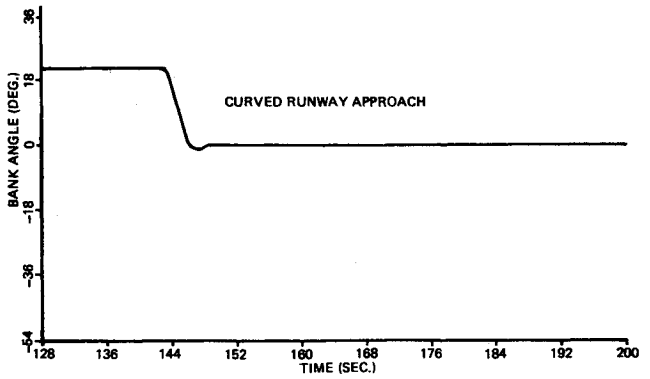

Fig. 9 Aircraft bank angle, simulated data, no noise.

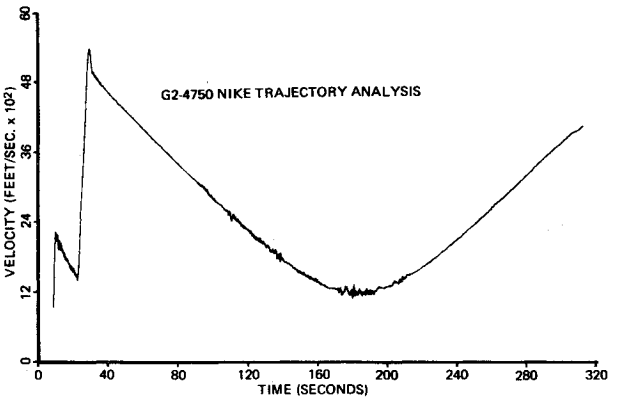

Fig. 11 Missile velocity, adaptive.

and estimates the state using

$$X_{n/n} = X_{n/n-1} + H_n(Y_n - M_n X_{n/n-1}) \tag{18}$$

Substituting Eqs. (15–17) into Eq. (18), an expression for the estimation error can be derived as

$$X_n - X_{n/n} = (I - H_n M_n)[\Phi_{n/n-1}(X_{n-1} - X_{n-1/n-1}) + W_n] - H_n V_n - H_n K_n \gamma_n \tag{19}$$

Defining P_n as the partial derivative of the state estimation error with respect to the vector of nonobservable systematic errors

$$P_n = \partial(X_n - X_{n/n})/\partial\gamma \tag{20}$$

It can be shown that

$$P_n = (I - H_n M_n)\Phi_{n/n-1} P_{n-1} - H_n K_n \tag{21}$$

This is an extremely important result, in that P_n is the error in the estimate at the present time point n due to a unit value of the nonobservable systematic errors from time point zero through time point n, with $P_o = 0$. All of the terms in Eq. (21) are already computed in the filter except $H_n K_n$. Note that P_n is independent of the value of the nonobservable systematic errors themselves. By mechanizing Eq. (21) in KAPPA, the error in the KAPPA estimate at each time point due to unit values of nonobservable systematic errors since time zero is known also.

The KAPPA covariance matrix computation can be augmented to account for nonobservable systematic error uncertainties also. The true covariance estimate is obtained by postmultiplying both sides of Eq. (19) by their transposes and taking expected values. An equivalent and less laborious result can be obtained by simply noting (as in Ref. 4) that P_n is effectively the matrix which transforms the nonobservable systematic error uncertainties into the state variable coordinates. Thus:

$$\Delta S_{n/n} = P_n \operatorname{var}\gamma P_n^T \tag{22}$$

where var γ is an a priori covariance matrix of the nonobservable systematic error uncertainties. The total covariance matrix then becomes:

$$S_{n/n} + \Delta S_{n/n} \tag{23}$$

Now that the total covariance matrix, including the effects of nonobservable systematic errors, is known, it would of course be possible to reformulate the Kalman gain equation in terms of $S_{n/n}$ and $\Delta S_{n/n}$ to account for their presence. This is not done in KAPPA, and consequently KAPPA is suboptimal if nonobservable systematic errors are present. The expected value of these errors is zero (due to routine calibration of the Wallops radars), however, and Eqs. (21) and (22) permit ready calculation of the error in the estimate as formulated. Furthermore, the high data rate of the radars means that a measurement bias has virtually no effect on other than position estimates, and then only on the order of the bias itself.

Typical Results

The KAPPA program was coded in FORTRAN IV on the NASA Wallops Island HW-625 computer. The original version was built into a postmission data analysis program in double precision having a proliferation of options and auxiliary parameters. The basic filter equations were then reprogramed for real-time operations in a streamlined single precision version. Except for the auxiliary computation of bias error propagation, the mathematical exactness of the real-time version is the same. This version of KAPPA requires approximately 8000 words of memory and cycles in 25 msec on the HW-625.

Figures 3, 4, and 5 show a typical MPS-19 radar track of an airplane, analyzed by the KAPPA program. This data set demonstrates the ability of the program to extract higher order

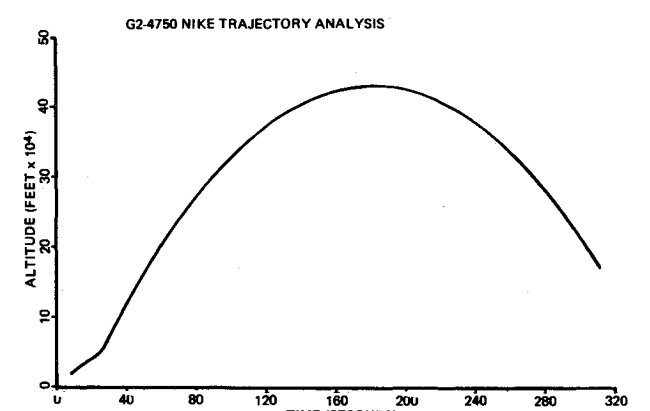

Fig. 10 Missile altitude.

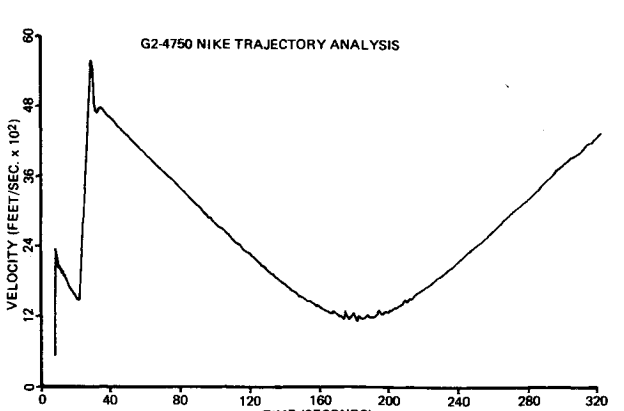

Fig. 12 Missile velocity, nonadaptive.

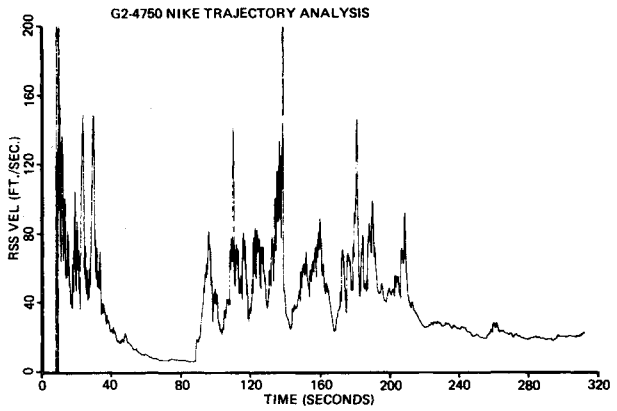

Fig. 13 Missile velocity standard deviation, adaptive.

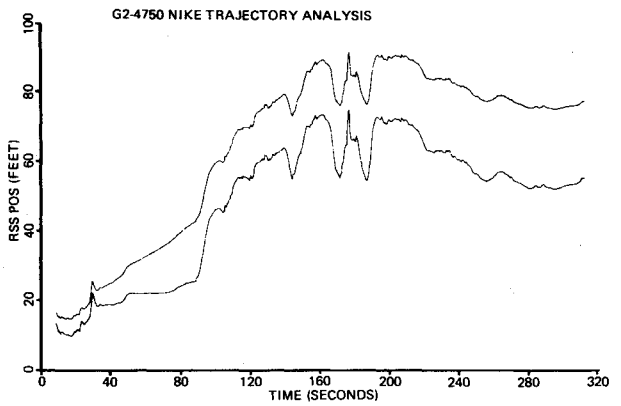

Fig. 15 Missile position standard deviation, error analysis mode.

terms, such as bank angle, from a high noise tracker (MPS-19) and at a slow data rate (one point per two secs). Note the correlation between the turn in the X-Y plot (Fig. 3), the change in flight azimuth, or heading (Fig. 4), and the dip in bank angle (Fig. 5).

In order to evaluate the accuracy and lag characteristics of KAPPA, it was necessary to use simulated data. A simulator was developed with which range, azimuth, and elevation measurements from a variety of trajectories could be computed with a selectable amount of random noise. The X-Y plot of a typical aircraft pattern appears in Fig. 6.

The aircraft pattern was generated to simulate a constant bank angle during the turn, and the transition from straight and level to turning flight was instantaneous. Figure 7 displays the computed bank angle leaving the turn. This plot was from a run made with a high degree of adaptability in the filter. The lag following the transition is minimal, but the penalty for filter transient response is paid by relatively high noise in the computed bank angle.

Figure 8 displays the effect (using the same input noise) of using less adaptability in the filter. The noise on the bank angle has been significantly reduced, but with loss of filter response. This tends to be a classic problem in data analysis, and the most optimum operation of the filter must be determined from the user's a priori knowledge of the data set and the desirability of smooth data vs filter response.

Figure 9 displays the filter response to noisless measurements. The noted lag is due to bank angle being a higher-order term, and to measurement weights that assumed a moderate amount of noise.

The error analysis and the missile tracking capabilities of KAPPA are displayed in Figs. 10–15. These plots were taken from two KAPPA runs (adaptive and nonadaptive) of an FPS-16 radar track of a NIKE missile fired from Wallops Island. The trajectory analysis begins shortly after first stage burn-out, is followed through second stage ignition and burn-out, and then well past apogee (see altitude vs time, Fig. 10).

The purpose of the launch was to fire a series of grenades beginning at $T+90$ secs in the flight. The result of the grenade launches is evident in the following plots.

Figures 11 and 12 are the velocity plots from the adaptive and nonadaptive runs, respectively. The advantage of the adaptive mode is most evident in the second stage burn-out (approximately $T+28$ secs). The nonadaptive mode displays more overshoot, and then undershoots.

Figures 13 and 14 display the rss velocity standard deviations for the adaptive and nonadaptive modes, respectively. Note that Fig. 14 is the error propagation due to geometry only, whereas Fig. 13 displays the results of unmodeled fluctuations in the data, i.e., the grenades firing. In addition, each peak in Fig. 13 corresponds to the expected firing times of the grenades. The hump in Fig. 14 at approximately 200 secs is due to the transition of determination of the velocity vector from the range measurement to the elevation measurement.

Figure 15 displays the rss position standard deviations for an error analysis run. The lower trace is the error propagation assuming a fixed amount of random noise on the measurements. The upper trace is the propagation of noise plus a nominal amount of measurement bias on range, azimuth, and elevation.

Figures 16–18 display a recent application of KAPPA, and suggest some modifications to enhance KAPPA's capabilities. The plots are of FPQ-6 radar tracks of two super-critical designed fuselages that were air-dropped at Wallops. The aerodynamic design was expected to exhibit a minimum drag effect while passing through Mach 1. Figure 16 displays acceleration vs velocity from the normal R, A, E measurements processed by KAPPA. The resulting noise relative to the desired parameter fluctuation at Mach 1 in this run was much too high.

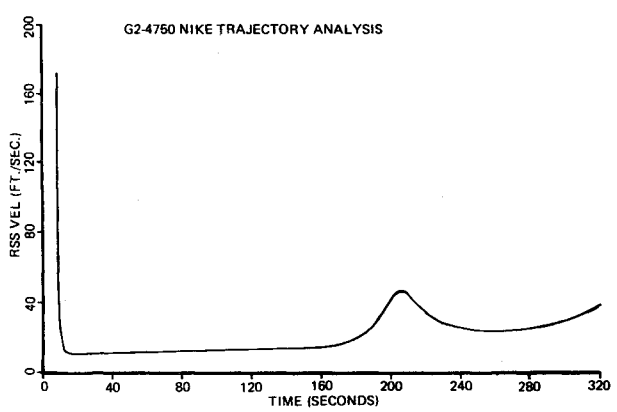

Fig. 14 Missile velocity standard deviation, nonadaptive.

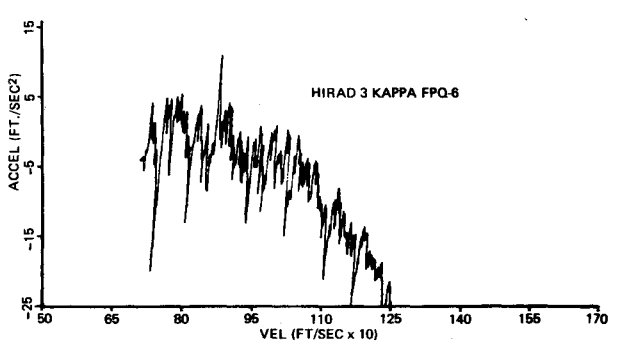

Fig. 16 Supercritical body no. 3 acceleration, R, A, E.

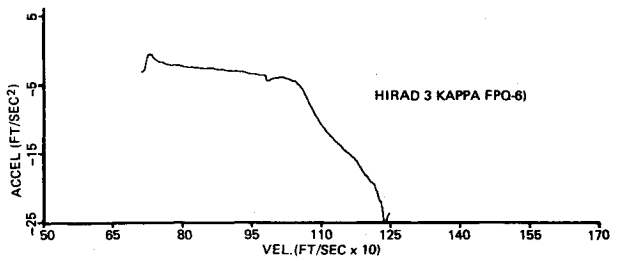

Fig. 17 Supercritical body no. 3 acceleration, $\dot{R}$, A, E.

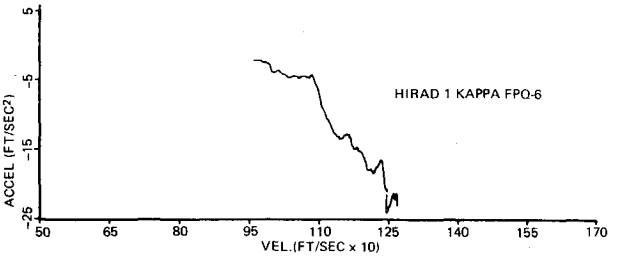

Fig. 18 Supercritical body no. 1 acceleration, $\dot{R}$, A, E.

Fortunately a more accurate measurement parameter is available with the FPQ-6 radar—doppler range-rate. The experiment was designed so that the vehicle was released in a trajectory heading at the radar, thereby maximizing the velocity fluctuations in the range-rate measurements. The precision doppler measurements were then integrated to yield range, and processed by KAPPA along with the standard azimuth and elevation. The resulting enhancement is displayed in Fig. 17, made from the same drop as Fig. 16. (The small fluctuation at approximately 100 sec is due to a "glitch" in the doppler data.) Further verification of the expected drag reduction was obtained by processing a different test (Fig. 18). The results of this analysis indicated the desirability of range-rate as a parameter in the measurement vector, and this modification is currently in progress.

Conclusions

The development and evaluation of KAPPA has shown the feasibility of applying a single Kalman filter program to both real-time traffic management and postmission analysis problems at the NASA Wallops Test Range. It has been possible to build in the versatility necessary to handle both aircraft and missile tracking applications in a single program, and to provide an error analysis capability without prohibitively increasing the program cycle time for real-time applications. Several improvements, which will enhance KAPPA's versatility and value as an operational tracking range software tool, have been identified and can be added in the future while remaining within a reasonable computer core and cycle time budget.

References

[1] Morrison, N., *Introduction to Sequential Smoothing and Prediction,* McGraw-Hill, New York, 1969.

[2] Hatfield, J. R. et al., "Suboptimal Linear Filtering with a Limited State," *AIAA Journal,* Vol. 9, No. 4, April 1971, pp. 747–749.

[3] McRary, J. W., "Detection of Unmodeled Errors in Recursive Trajectory Estimation," *AIAA Journal,* Vol. 7, No. 9, Sept. 1969, pp. 1790–1792.

[4] Martin, C. F., "Error Analysis of Statistical Techniques Used in Orbit Estimation," June 1969, Wolf Research and Development Corp., Riverdale, Md.

JULY 1973 AIAA JOURNAL VOL. 11, NO. 7

Mathematical Formulation of Viscous-Inviscid Interaction Problems in Supersonic Flow

GABRIEL MILLER*
New York University, Bronx, New York

The problem area of the interaction between the viscous and inviscid flowfields around a body is investigated. A flow model is presented which can determine interaction effects without the possibility of having to choose between an infinite number of possible solutions. The importance of the inclusion of a two-family characteristic net for the outer supersonic flow and the normal momentum equation for the inner viscous flow is discussed as is the necessity of their inclusion for a properly posed model problem leading to a unique solution. A result of the numerical analysis based on the flow model is presented and the uniqueness of such results is discussed.

I. Introduction

MUCH attention has been devoted over the past two decades to the problem area of the interaction between the boundary-layer flow and the "inviscid" flow over a body in high-speed flight. Significant changes in the pressure field associated with the boundary-layer displacement at moderate Reynolds number or changes in boundary-layer profiles associated with large entropy gradients created by blunt bodies at high Mach numbers can only be accommodated by a theory whose framework includes the effects of interaction.

When the boundary layer is relatively thick (i.e. at low or moderate Reynolds numbers) the approximation of zero normal pressure gradient loses validity, and thus analyses which include the effects of interaction must include the second momentum equation in the viscous layer. This effect, coupled with the match-

Received September 7, 1972; revision received March 15, 1973. The work reported herein was supported by the Department of the Navy, Office of Naval Research, under Contract N00014-67-A-0467-0021.

Index categories: Boundary Layers and Convective Heat Transfer—Laminar; Jets, Wakes, and Viscid-Inviscid Flow Interactions.

* Assistant Professor of Aeronautics and Astronautics. Member AIAA.